Hydrogen and carbon black production from thermal decomposition of sub-quality natural gas

by

M. Javadi and M. Moghiman

reprinted from

International journal of spray and combustion dynamics

Volume 2 • Number 1 • 2010

Multi-Science Publishing
ISSN 1756-8277

Hydrogen and carbon black production from thermal decomposition of sub-quality natural gas

M. Javadi[1] and M. Moghiman

Department of mechanical engineering, Ferdowsi University of Mashhad, Iran

P. O. Box:91775-1111

mohammad.javadi@gmail.com, mmoghiman@yahoo.com

Received December 26, 2008; Accepted June 01, 2009

ABSTRACT

The objective of this paper is computational investigation of the hydrogen and carbon black production through thermal decomposition of waste gases containing CH_4 and H_2S, without requiring a H_2S separation process. The chemical reaction model, which involves solid carbon, sulfur compounds and precursor species for the formation of carbon black, is based on an assumed Probability Density Function (PDF) parameterized by the mean and variance of mixture fraction and β-PDF shape. The effects of feedstock mass flow rate and reactor temperature on hydrogen, carbon black, S_2, SO_2, COS and CS_2 formation are investigated. The results show that the major factor influencing CH_4 and H_2S conversions is reactor temperature. For temperatures higher than 1100° K, the reactor CH_4 conversion reaches 100%, whilst H_2S conversion increases in temperatures higher than 1300° K. The results reveal that at any temperature, H_2S conversion is less than that of CH_4. The results also show that in the production of carbon black from sub-quality natural gas, the formation of carbon monoxide, which is occurring in parallel, play a very significant role. For lower values of feedstock flow rate, CH_4 mostly burns to CO and consequently, the production of carbon black is low. The results show that the yield of hydrogen increases with increasing feedstock mass flow rate until the yield reaches a maximum value, and then drops with further increase in the feedstock mass flow rate.

Key words: Hydrogen, carbon black, sulfur compounds, thermal decomposition, sour natural gas

1. INTRODUCTION

As the prices of fossil fuel increase, abundant sour natural gas, so called sub-quality natural gas (SQNG) resources become important alternatives to replace increasingly exhausted reserves of high quality natural gases for the production of carbon black, hydrogen, sulfur and/or CS_2 [1–3]. At oil flow stations it is common practice to flare or vent

[1]Corresponding author. Fax: 0098-511-8763304
E-mail address: Mohammad.Javadi@gmail.com

SQNG, which is produced along with crude oil. This accounts for more than 100 million cubic meters (m^3) world-wide per day, and approximately equals to France's annual gas consumption [4]. Clearly this is of considerable concern in terms of global resource utilization and climate change implications. Gas flaring has also been blamed for environmental and human health problems such as acid rain, asthma, skin and breathing diseases [5]. The removal of H_2S from SQNG is expensive and not commercially viable for large-scale plants. When H_2S concentration in natural gas is higher than about 1.0%, the high separation cost makes the SQNG uneconomical to use [1]. As mentioned above, production of carbon black from SQNG is one viable option utilizing this untapped energy resource while at the same time reducing carbon oxides and hydrogen sulfide emissions. In a carbon black furnace, thermal decomposition of $CH_4 + H_2S$ produces hydrogen, carbon and other sulfur compounds [6]. Hydrogen is a promising candidate as a clean energy carrier. It is increasingly recognized as an efficient and sustainable fuel of the future as it is a preferred fuel for fuel cells in homes and cars [7]. Eventual realization of a hydrogen economy requires cost effective and readily available hydrogen containing feedstocks and viable technologies for extracting high purity H_2 [8]. Methane as the main component of sub quality natural gas can be converted to hydrogen and carbon in a carbon black gas furnace [8, 9].

Carbon black is an industrial form of soot produced by subjecting hydrocarbon feedstock to extremely high temperatures in a carefully controlled combustion process [9]. Carbon black is widely used as filler in elastomers, tires, plastics and paints to modify the mechanical, electrical and optical properties of materials in which it is used [10, 11].

The purpose of this paper is to assess production of hydrogen and carbon black from sub-quality natural gas (SQNG) using a 3D numerical technique that employs a detailed turbulent flame structure leading to production of hydrogen, carbon black and sulfur compounds. Formation of carbon black is associated with both specific pyrolysis species and soot formation during incomplete combustion of natural gas. The effect of relevant process parameters such as feed gas mass flow rate and reactor temperature on hydrogen, carbon black, S_2, SO_2, COS and CS_2 formation have been described.

2. GAS FURNACE CARBON BLACK AND THERMAL DECOMPOSITION OF SQNG

The carbon black furnace used in this investigation is a small-scale axial flow reactor identical to that reported previously by Gruenberger [4]. The furnace has been designed on the basis of using gaseous fuels as feedstock hydrocarbon, with a maximum output of 10 kg carbon black per hour. The basic geometry of the carbon black furnace is shown in Fig. 1, consisting of a precombustor, a mixing zone and a reactor. In the precombustor, the axially injected natural gas burns with inlet air introduced through two tangential inlets. Then, the highly swirling hot combustion gases mix with the sub-quality natural gas injected radially into the precombustor in the proximity of the mixing zone. A sudden increase in the tube diameter at the exit of the choke promotes vigorous mixing of the SQNG fuel with the hot gases leading to thermal decomposition of $CH_4 + H_2S$ and formation of hydrogen, carbon black, sulfur compounds and other precursor species for the formation of carbon black [11].

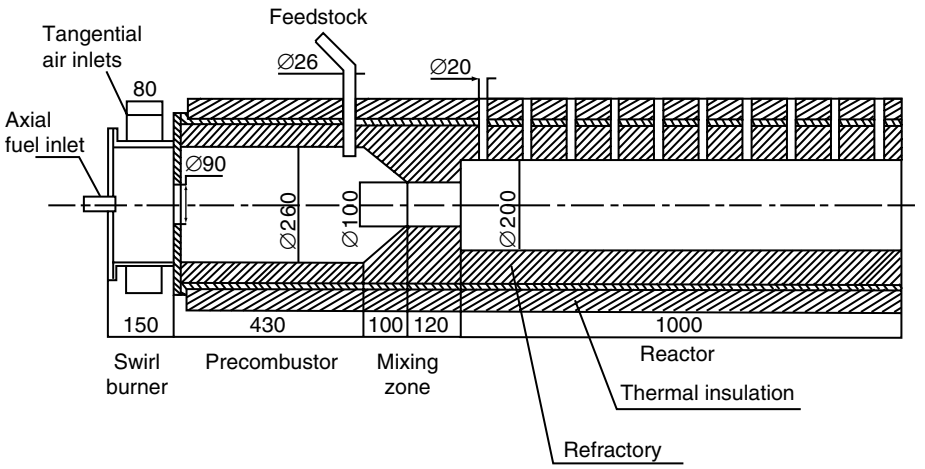

Figure 1: Carbon black gas furnace.

3. CHEMICAL REACTION MODELING

Production of carbon black through thermolysis of SQNG involves a complex series of chemical reactions which control conversion of both CH_4 and H_2S as follows [3, 12]:

$$CH_4 \rightarrow C(S) + 2H_2 \qquad \Delta H^{\circ}_{298} = -74.9\,\text{kJ / mol} \qquad \text{Reaction (1)}$$

$$H_2S \rightarrow \frac{1}{2}S_2 + H_2 \qquad \Delta H^{\circ}_{298} = -79.9\,\text{kJ / mol} \qquad \text{Reaction (2)}$$

Since reaction 1 is mildly endothermic, it requires temperatures higher than 850°K to proceed at reasonable rates [13], and, as reaction 2 is highly endothermic, temperatures in excess of 1500°K are required for achieving reasonable rates [6]. A portion of CH_4 and H_2S can oxidize to produce CO, CO_2 and SO_2. H_2S can also react with CO_2 producing COS [14]:

$$H_2S + CO_2 \Leftrightarrow COS + H_2O \qquad \text{Reaction (3)}$$

Under special circumstances including using catalyst H_2S can react with methane producing carbon disulfide (CS_2) and H_2 [3].

$$2H_2S + CH_4 \Leftrightarrow CS_2 + 4H_2 \qquad \Delta H^{\circ}_{298K} = 232\,\text{kJ/mol} \qquad \text{Reaction (4)}$$

4. TURBULENCE–CHEMISTRY INTERACTION

The mixture fraction/PDF method is used to model the turbulent chemical reactions occurring in the diffusion, combustion and thermal decomposition of natural gas in the

carbon black furnace. This method, which assumes the chemistry is fast enough for a chemical equilibrium to always exist at molecular level, enables handling of large numbers of reacting species, including intermediate species. Transport equations are solved for the mean mixture fraction $\bar{f}$, its variance $\overline{f'^2}$ and for enthalpy $\bar{h}$. Calculations and PDF integrations are performed using a preprocessing code, assuming chemical equilibrium between 30 different species. The results of the chemical equilibrium calculations are stored in look-up tables which relate the mean thermochemical variables (species mass fractions, temperature and density) to the values of $\bar{f}$, $\overline{f'^2}$ and $\bar{h}$ [15].

In non-adiabatic systems, where change in enthalpy due to heat transfer affects the mixture state, the instantaneous thermo chemical state of the mixture, resulting from the chemical equilibrium model, is related to a strictly conserved scalar quantity known as the mixture fraction, f, and the instantaneous enthalpy, H^*, $\phi_i = \phi_i(f, H^*)$. The effects of turbulence on the thermo chemical state are accounted for with the help of a probability density function (PDF):

$$\bar{\phi}_i = \int_0^1 \phi_i(f, \bar{H}^*) p(f) df. \tag{1}$$

In this work, the β-probability density function is used to relate the time-averaged values of individual species mass fraction, temperature and fluid density of the mixture to instantaneous mixture fraction fluctuations. The β-PDF in terms of the mean mixture fraction $\bar{f}$ and its variance $\overline{f'^2}$, can be written as:

$$P(f) = \frac{f^{\alpha-1}(1-f)^{\beta-1}}{\int_0^1 f^{\alpha-1}(1-f)^{\beta-1} df}, \quad 0 < f < 1 \tag{2}$$

where:

$$\alpha = \bar{f}\left[\frac{\bar{f}(1-\bar{f})}{\overline{f'^2}} - 1\right], \beta = (1-\bar{f})\left[\frac{\bar{f}(1-\bar{f})}{\overline{f'^2}} - 1\right]. \tag{3}$$

Using the unweighted averaging [16], the values of the two parameters $\bar{f}$ and $\overline{f'^2}$ at each point in the flow domain are computed through the solution of the following conservation equations [17]:

$$\frac{\partial}{\partial x}(\rho u_i \bar{f}) = \frac{\partial}{\partial x_i}\left(\frac{\mu_t}{\sigma_t}\frac{\partial \bar{f}}{\partial x_i}\right), \tag{4}$$

$$\frac{\partial}{\partial x}(\rho u_i \overline{f'^2}) = \frac{\partial}{\partial x_i}\left(\frac{\mu_t}{\sigma_t}\frac{\partial \overline{f'^2}}{\partial x_i}\right) + C_g \mu_t \left(\frac{\partial \bar{f}}{\partial x_i}\right)^2 - C_d \rho \frac{\varepsilon}{k}\overline{f'^2}, \tag{5}$$

where the constants σ_t, C_g (= $2/\sigma_t$) and C_d take the values 0.7, 2.86 and 2.0, respectively. The distribution of the instantaneous enthalpy is calculated from a transport equation as follows:

$$\frac{\partial}{\partial x}(\rho u_i \overline{H^*}) = \frac{\partial}{\partial x_i}\left(\frac{k_t}{c_p}\frac{\partial \overline{H^*}}{\partial x_i}\right) + \tau_{ik}\frac{\partial u_i}{\partial x_k} + S_h \tag{6}$$

where k_t is turbulent thermal conductivity and S_h includes the heat generated by the chemical reaction and radiation. The instantaneous enthalpy is defined as:

$$H^* = \sum_j m_j H_j = \sum_j m_j \left[\int_{T_{ref,j}}^{T} c_{p,j} dT + h_j^{\circ}(T_{ref,j})\right] \tag{7}$$

where m_j is the mass fraction of species j and h_j° ($T_{ref,j}$) is the formation enthalpy of species j at the reference temperature $T_{ref,j}$.

5. SOOT FORMATION MODEL

Here, soot formation is modeled by that proposed by Brooks and Moss [18]. The model describes the soot formation in terms of soot particle number density (N) and the mass density (M) and taking into account the inception (nucleation), coagulation, growth and oxidation on the rates as follows:

$$\frac{DN}{Dt} = \left(\frac{dN}{dt}\right)_{Inception} + \left(\frac{dN}{dt}\right)_{Coagulation} \tag{8}$$

And

$$\frac{DM}{Dt} = \left(\frac{dM}{dt}\right)_{Inception} + \left(\frac{dM}{dt}\right)_{Growth} + \left(\frac{dM}{dt}\right)_{Oxidation} \tag{9}$$

The acetylene inception model is used for the calculation of soot inception rate according to Brookes & Moss [18]. The inception rates are computed by:

$$\left(\frac{dN}{dt}\right)_{Inception} = c_1 N_A \left(\rho \frac{m_{C_2H_2}}{W_{C_2H_2}}\right) e^{-21100/T} \tag{10}$$

and

$$\left(\frac{dM}{dt}\right)_{Inception} = \frac{M_P}{N_A}\left(\frac{dN}{dt}\right)_{Inception} \tag{11}$$

where M_p, the mass of a soot nucleus, has a value of 144 kg kmol^{-1} based on the assumption that the soot size corresponds to 12 carbon atoms and $c_1 = 54$ s^{-1} determined by Brookes and Moss [18].

Assuming that particles are monodispersed in size and are spherical, the coagulation rate and reaction surface are given by:

$$\left(\frac{dN}{dt}\right)_{coagulation} = -\left(\frac{24R}{\rho_{Soot} N_A}\right)^{1/2} \left(\frac{6}{\pi \rho_{Soot}}\right)^{1/6} T^{1/2} M^{1/6} N^{11/6} \tag{12}$$

and

$$\left(\frac{dM}{dt}\right)_{growth} = c_2 \left(\rho \frac{m_{C_2H_2}}{W_{C_2H_2}}\right) e^{-21100/T} \times \left((\pi N)^{1/3} \left(\frac{6M}{\rho_{Soot}}\right)^{2/3}\right) \tag{13}$$

Where R is the universal gas constant, $\rho_{soot} = 2000\,kg.m^{-3}$ and $c_2 = 9000.6\,kg.m.kmol^{-1}.s^{-1}$ according to Wen et al. [19].

6. SOOT COMBUSTION MODEL

Soot oxidation is modeled by using O_2–OH oxidation model [19]. This model takes into account oxidation of soot by both O_2 and OH radicals. The rate of soot oxidation is given by [19, 20]:

$$\begin{aligned}\left(\frac{dM}{dt}\right)_{Oxidation} = & -c_4 \rho \eta \frac{m_{OH}}{W_{OH}} \sqrt{T} (\pi N)^{1/3} \left(\frac{6M}{\rho_{Soot}}\right)^{\frac{2}{3}} \\ & -c_3 \rho \frac{m_{O_2}}{W_{O_2}} \exp\left(\frac{-19778}{T}\right) \sqrt{T} (\pi N)^{1/3} \left(\frac{6M}{\rho_{Soot}}\right)^{2/3}\end{aligned} \tag{14}$$

where $\eta = 0.13$ and $c_4 = 105.81$ kg.m.kmol^{-1}.K$^{-1/2}$.s^{-1}, which are obtained by converting the rate of soot consumption.

7. NUMERICAL SOLUTION PROCEDURE

Fluent CFD software has been used to model the furnace employing solution-adaptive grid refinement technique to solve the 3D problem. Gambit preprocessor is used for the fully three dimensional geometry creation and unstructured grid generation. The 3D volume grid is represented in Fig 2. The domain is discretized into a grid of 20493 nodes and 82745 tetrahedral cells. The conservation equations for mass, momentum, energy, Reynold's stresses, dissipation rate, mixture fraction and its variance, and concentration of soot are solved by finite-volume analysis, using a second-order upwind scheme for discretisation of the convective terms in the transport equations.

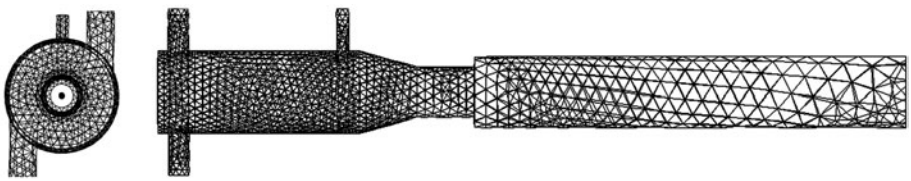

Figure 2: Three-dimensional tetrahedral grid.

The acetylene inception soot model is implemented via user-defined functions within the finite-volume CFD code FLUENT. The radiative heat transfer in the absorbing, emitting and scattering medium is calculated by the Discrete Ordinates (DO) radiation model [21]. The RSM model is used for prediction of anisotropic, highly swirling and recirculating flow inside the combustor. Abandoning the isotropic eddy-viscosity hypothesis, the RSM closes the Reynolds-averaged Navier-Stokes equations by solving six differential transport equations for Reynolds stresses, together with an equation for the dissipation rate of turbulence kinetic energy. The conventional wall-function approach is used in the near-wall region. At the inlet boundary, conditions are specified once and did not need updating during the course of the solution procedure. At the outlet boundary, zero gradient conditions are applied. We assumed an isothermal boundary condition at the wall of the furnace.

A grid dependence study was conducted to arrive at the appropriate size of the grid for optimal accuracy and efficiency. The number of grid points was varied from 17231 to 36387 for typical set operating conditions. We observed that the field quantities varied less than 1% after the number of grid points increased beyond 20493. For the radiation model, emissivity coefficient at the flow inlets and outlets were taken to be 1.0 (black body absorption). Wall emissivity was set at 0.6, a typical value for combustion gases.

8. RESULTS

Numerical calculations were performed on the axial flow gas furnace described by Gruenberger [4] as shown in Fig. 1. The total precombustor inlet airflow rate is $19 \times 10^{-3}\ m^3/s$, at a temperature of 690°K and pressure of 1 bar. The equivalence ratio used for the precombustor is 0.92. The accuracy of the quantitative or even the qualitative trends for the combustion and decomposition parameters depend on the accuracy with which the temperature and species concentration fields are determined from the numerical calculation of the present model. To establish the accuracy of our model, we calculated and compared the model predictions to the experimental measurements of Gruenberger [4] with no H_2S. For comparison purposes, we first conducted computations without H_2S in feed gas.

A comparison of reactor outlet average temperature and carbon black yield (kg carbon black/kg feedstock) predicted by this model and that from experimental results is given in Figs. 3 and 4. Resulting of Fig. 3 depict that model predicts lower temperatures than the experimental data especially at high feed flow rates. The discrepancy

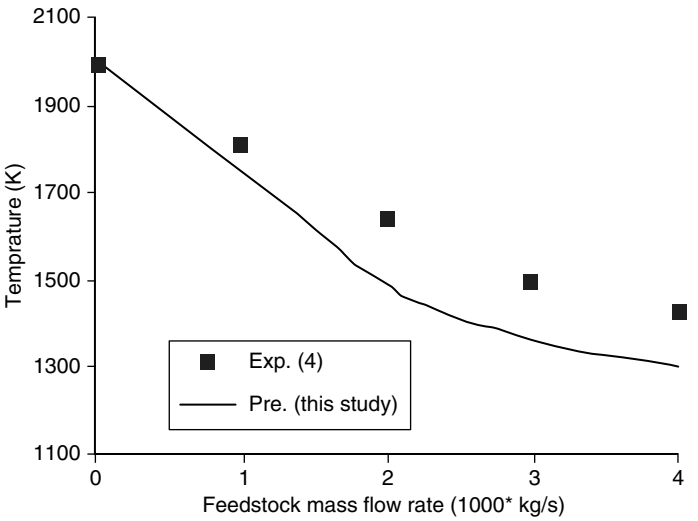

Figure 3: Comparison of the predicted reactor outlet temperature with the experimental data.

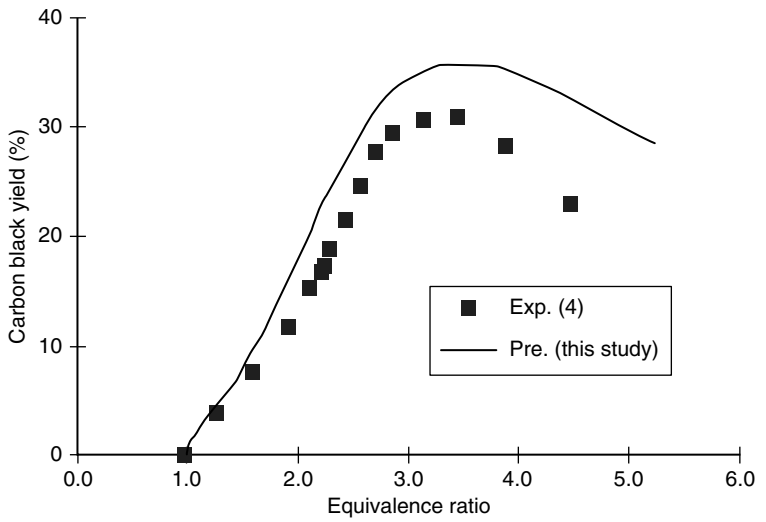

Figure 4: Comparison of the predicted carbon black yield with the experimental data.

between the two results might be due to the fundamental assumption made in the combustion model used (PDF fast chemistry combustion model) which assumes that chemistry is fast enough for a chemical equilibrium. Figure 4 show that the predicted and measured carbon black yields are in very good agreement and maximum carbon

black yield is reached at the equivalence ratio of 3. The discrepancy between the two results can be attributed to the temperature levels obtained by the two methods (see Fig. 3). The lower temperature levels computed by the model might be due to higher decomposition of CH_4. Figure 5 presents the calculated distributions for CH_4, H_2S, temperature and mass fraction of soot, carbon black, COS and gaseous sulfur predicted by the model at feed rate of 3×10^{-3} *kg/s*. H_2S mass fraction in natural gas assumed to be 10%. Of particular interest are Figs. 5d-f that show soot formation due to incomplete combustion of inlet methane and production of solid carbon and gaseous sulfur by thermolysis of methane- hydrogen sulfide jet interaction with hot surroundings. Results from the model calculations seem to indicate that the use of more inlet injection ports for SQNG feed would increase the yield of carbon black and sulfur compounds.

Figure 6 shows the reactor outlet temperature as a function of inlet mass flow rate for two cases a) with H_2S, b) without H_2S. It can be seen that the results obtained for these two cases are similar. The small discrepancy between the results may be due to CH_4 decomposition reaction that begins at lower temperatures that of H_2S. Also, Fig. 6 depicts that temperatures drop precipitously with increasing flow rate of feed gas due to the endothermic nature of both CH_4 and H_2S decomposition reactions.

Figures 7 and 8 show the effect of feed gas flow rate and reactor outlet temperature on CH_4 and H_2S conversions given by [3]:

$$CH_4 \text{ conversion} = \frac{[CH_4]_0 - [CH_4]}{[CH_4]_0} \times 100, \; H_2S \text{ conversion} = \frac{[H_2S]_0 - [H_2S]}{[H_2S]_0} \times 100$$

where $[CH_4]_0$ and $[H_2S]_0$ denote the initial (input) concentration of CH_4 and H_2S, respectively. $[CH_4]$ and $[H_2S]$ are equilibrium concentration of CH_4 and H_2S at reactor outlet, respectively. Figure 7 depicts that the H_2S conversion drop sharply with increased feed gas flow rate; this can be attributed to the endothermic nature of H_2S and CH_4 decomposition reactions. For higher values of feed gas flow rate ($\geq$ 0.002kg/s) CH_4 conversion decreases with increased feed gas flow rate due to the endothermicity of CH_4 thermolysis. The major factor influencing CH_4 and H_2S conversions appears to be temperature. Figure 8 shows that CH_4 conversion reaches 100% at temperatures above 1100°K. Because CH_4 decomposition reaction is mildly endothermic, the temperature must be above 850°K for the reaction to proceed at a reasonable rate. This is in accord with the results of Huang and T-Raissi [3]. At any temperature, H_2S conversion is less than that of CH_4, especially at those below 1300°K wherein H_2S conversion is less than 5%. For higher values of reactor temperature ($\geq$1300°K), H_2S conversion increases sharply with reaction temperature. As H_2S decomposition reaction is endothermic, the temperature must be above 1500°K for the reaction to proceed at rapid rates.

Figure 9 shows the effect of feedstock flow rate on CH_4, carbon black, soot and CO mass fractions at the furnace outlet. It can be seen that for lower values of feed gas flow rates, the very high temperature precombustor effluent (see Fig. 6) causes the feedstock methane to convert to CO rather than carbon. For higher values of feedstock flow rate, the formation of carbon black increases, and due to the resulting lower temperatures, the mass fraction of CO and soot decreases. This is so because the soot model strongly

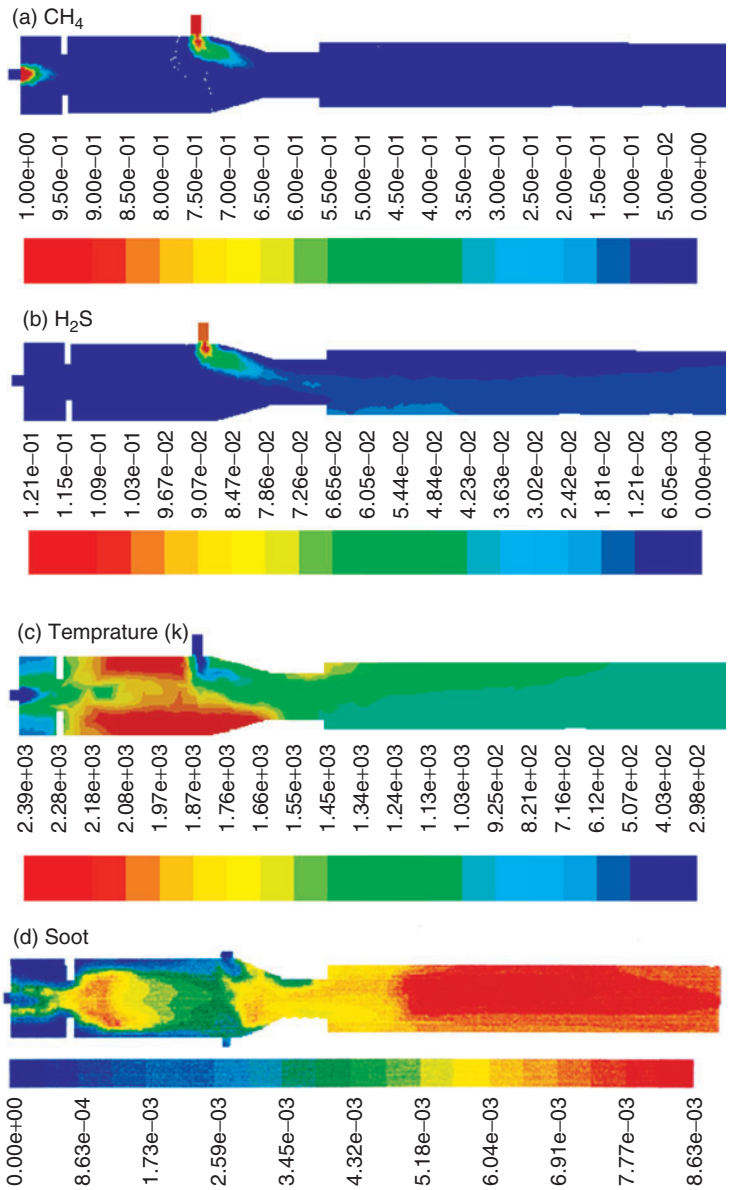

Figure 5 (*Continued*)

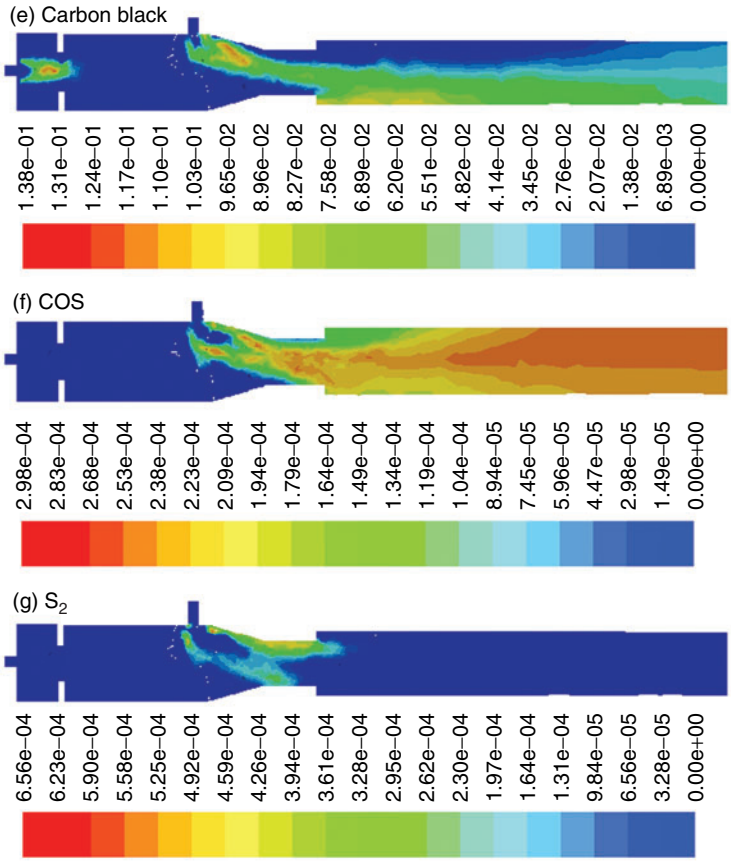

Figure 5: Contour of species mass fractions and temperature (K).

depends on the reaction temperature. Figure 10 shows the effect of feedstock flow rate on H_2 and carbon black yields at the furnace outlet. It can be seen that the yield of H_2 increases with increased feed gas flow rate until it reaches a maximum value, and then drop with further increase in the flow rate. For higher values of feedstock flow rate, the yield of carbon black increases, and, due to reduction in CH_4 conversion (see Fig. 7), the yield of hydrogen decreases.

Figure 11 depicts the yield of sulfur (due to H_2S decomposition) and SO_2 (due to H_2S combustion) as a function of feedstock flow rate at the outlet of the furnace. S_2 and SO_2 yields are defined as [3]:

$$S_2(\%) = \frac{2[S_2]}{[H_2S]_0} * 100,\ SO_2(\%) = \frac{[SO_2]}{[H_2S]_0} * 100.$$

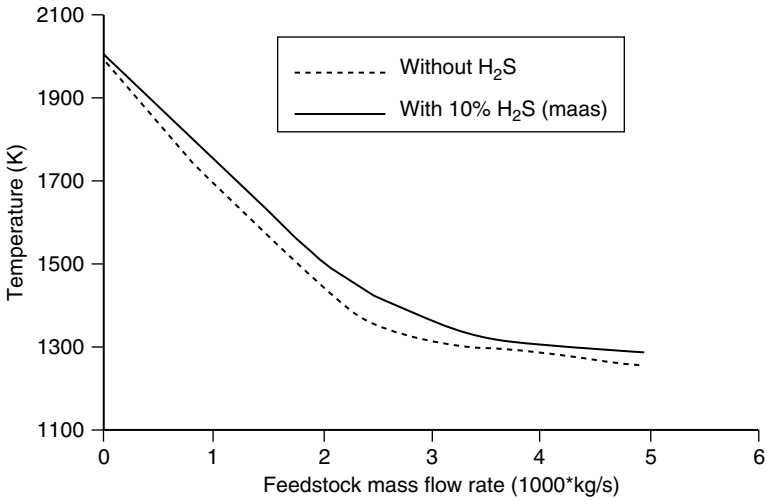

Figure 6: Effect of feedstock flow rate on calculated outlet temperature.

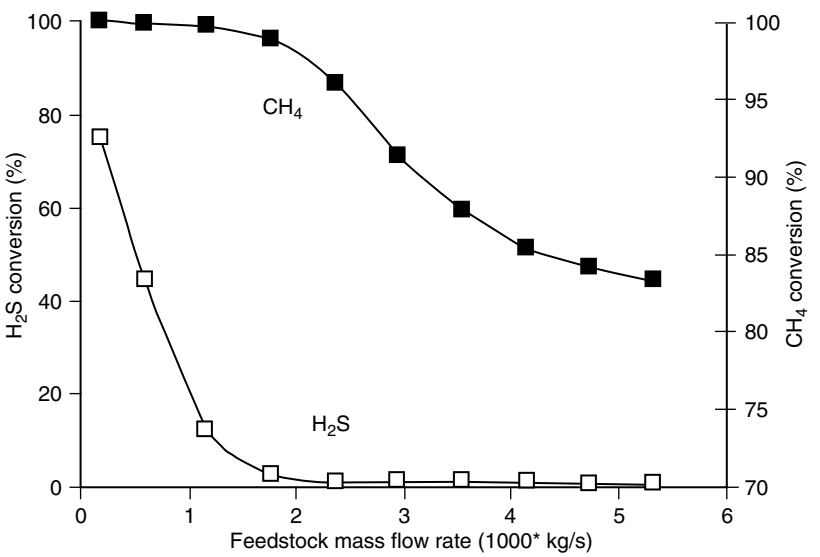

Figure 7: Effect of feedstock mass flow rate on H_2S and CH_4 conversions.

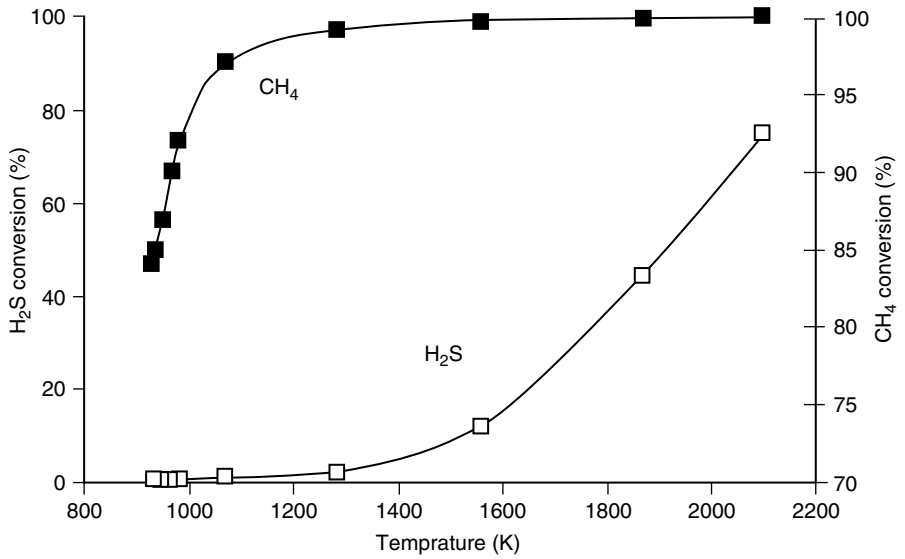

Figure 8: Effect of reactor outlet temperature on H_2S and CH_4 conversions.

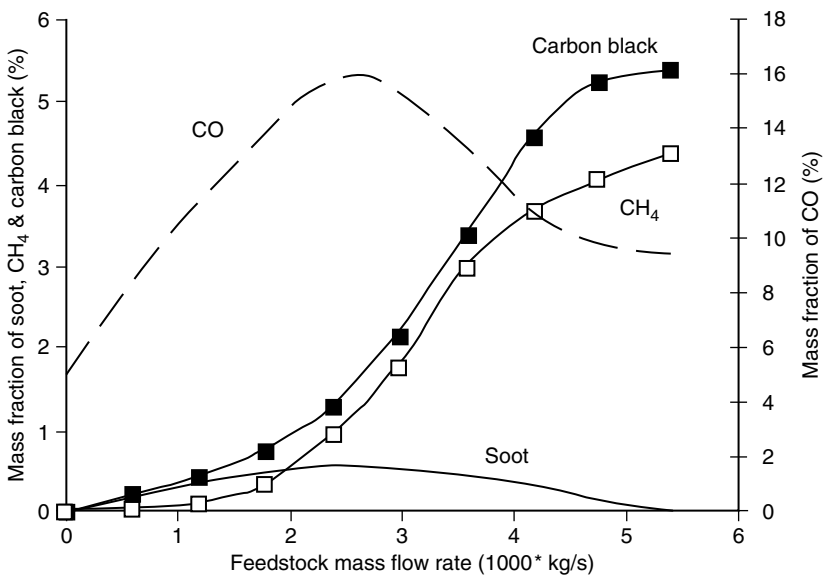

Figure 9: Effect of feedstock flow rate on CH_4, CO, carbon black, and soot mass fractions.

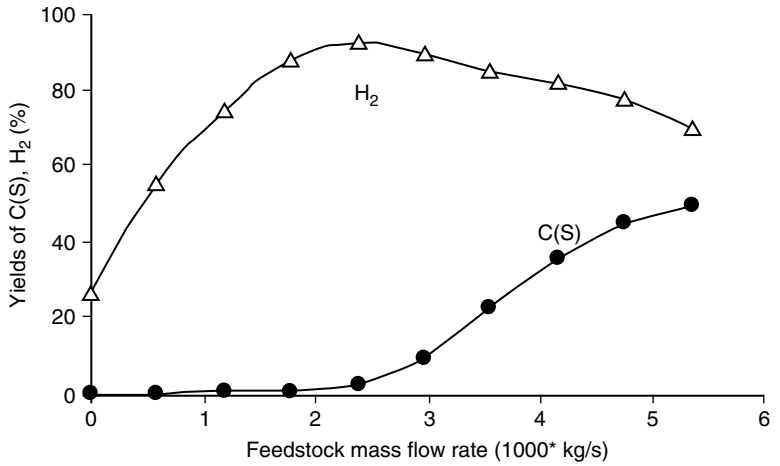

Figure 10: Effect of feedstock mass flow rate on H_2 and C(S) productions.

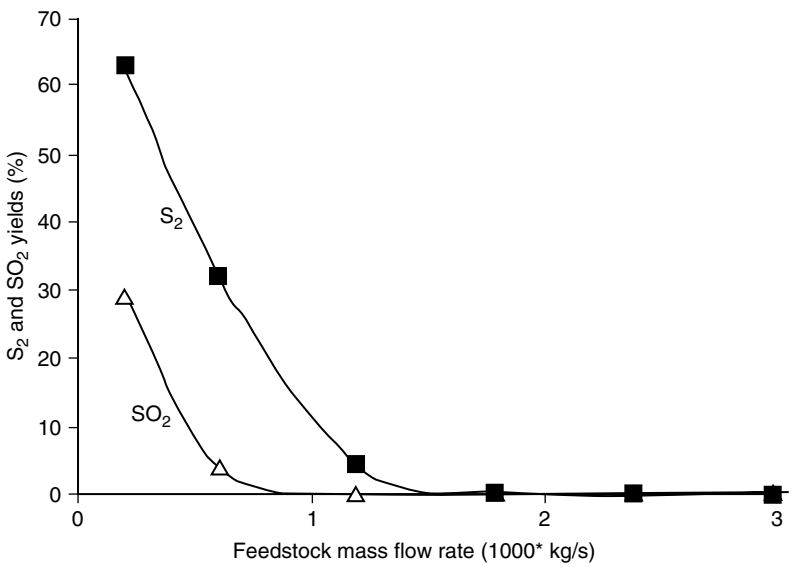

Figure 11: Effect of feedstock mass flow rate on S_2 and SO_2 .

where $[S_2]$ and $[SO_2]$ denote the equilibrium molar concentrations of S_2 and SO_2, respectively [8]. The figure reveals that for low values of feedstock flow rate (≤ 0.002kg/s) that result in high reaction temperatures (see Fig. 3) H_2S converts mostly to S_2 and SO_2. It can be seen that for higher values of feedstock flow rate, yield of S_2 and SO_2 are quite low. This is due to reduced conversion of H_2S conversion (see Figure

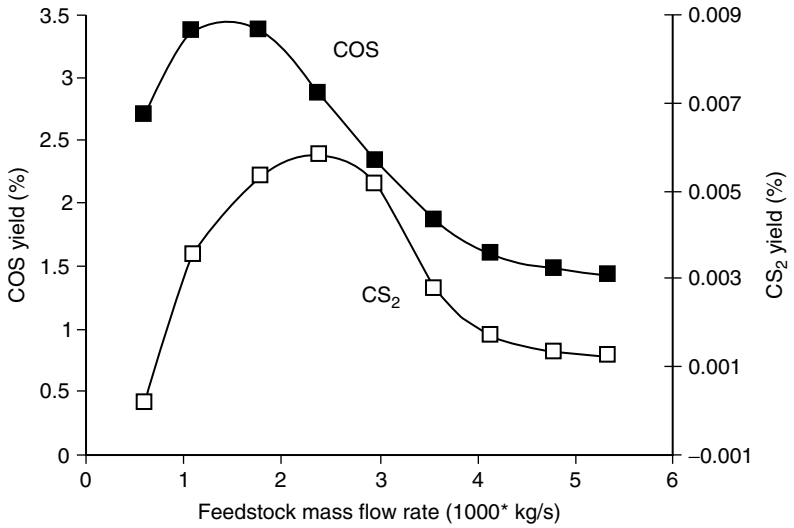

Figure 12: Effect of feedstock mass flow rate on *COS* and CS_2 yields.

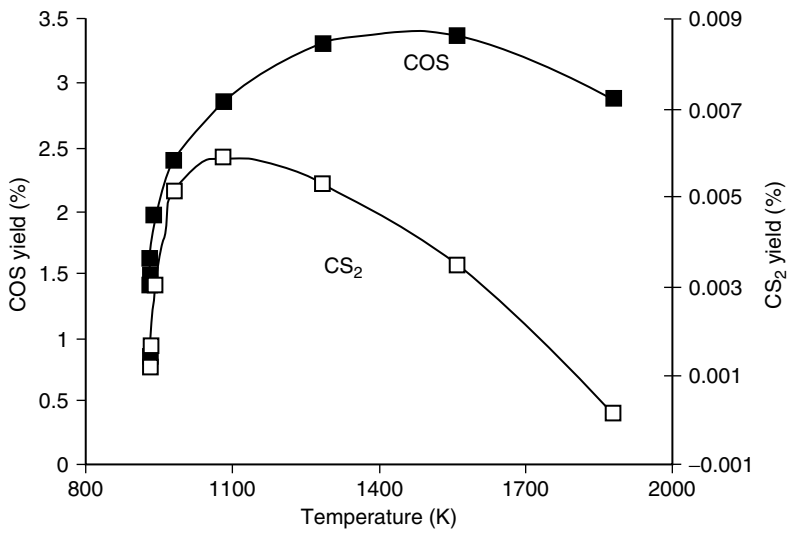

Figure 13: Effect of reactor outlet temperature on *COS* and CS_2 yields.

7). Figures 12 and 13 depict the effects of feedstock mass flow rate and temperature on the yield of COS and CS_2, respectively, as defined by:

$$\mathrm{COS}(\%) = \frac{[\mathrm{COS}]}{[\mathrm{H_2S}]_0} * 100,\ \mathrm{CS_2}(\%) = \frac{[\mathrm{CS_2}]}{[\mathrm{CH_4}]_0} * 100$$

where [COS] and [CS_2] denote the equilibrium molar concentration of COS and CS_2, respectively [3]. Figure 12 shows that COS and CS_2 yields increase with increased feedstock flow rate until they reach a peak, and then drop with further increase in feed gas flow rate. Figure 13 shows that the increase in temperature results in increased COS and CS_2 yield up to their respective maxima and then decrease. The maxima of COS and CS_2 yields occur at different temperatures (1100°K and 1300°K respectively). Figures 12 and 13 reveal that yield of CS_2 is always low (≤ 0.0007%). This is in accord with results of Huang and T-Raissi [3] and Towler and Lynn [12].

9. CONCLUSIONS

The production of hydrogen and carbon black from sub-quality natural gas containing methane (CH_4) and hydrogen sulfide (H_2S) has been analyzed. The process involved the oxidative and thermal decomposition of CH_4 with and without H_2S present. Based on the presented results, the following conclusions may be drawn:

- The major factor influencing CH_4 and H_2S conversions is the reactor temperature.
- At temperatures above 1100°K, CH_4 conversion is complete.
- At any temperature, H_2S conversion is less than that of CH_4, especially at temperature below 1300°K for which H_2S conversion is less than 5%.
- The yield of hydrogen increases with increasing feed gas mass flow rate until it peaks and then drops with further increase in the flow rate.
- For temperatures higher than 1300°K, H_2S conversion increases sharply with temperature. The major reaction products are S_2 and SO_2 with carbonyl sulfide (COS) and carbon disulfide (CS_2) being present as minor products.
- For lower values of feedstock flow rate, CH_4 is converted to mostly CO and consequently, the yield of carbon black is low. For higher values of feed gas mass flow rates yield of carbon black increases to a maximum value before dropping at much higher feed gas flow rates.

REFERENCES

[1] C. Huang, A. T-Raissi, *J. Power Sources,* 163, 645–652 (2007).

[2] H.K. Abdel, M.A. Shalabi, D.K. AL-Harbi and T. Hakeem, *Int. J. Hydrogen Energy*, 23, 457–462 (1998).

[3] C. Huang and A. T-Raissi, *J. Power Sources*, 175, 464–472 (2008).

[4] T.M. Gruenberger, M. Moghiman, P.J. Bowen and N. Syred, Combust. *J. Sci. and Tech.*, 174, 67–86, (2002).

[5] T.W. Lambert, V.M. Goodwin, D. Stefani and L. Strosher, *Int. J. Science of the Total Environmen*t, 367, 1–22 (2006).

[6] C. Huang and A. T-Raissi, *J. Power Sources*, 163, 637–644 (2007).

[7] H. Ryu, Y. Lee, H. Lee, Y. Han, J. Lee and J. Yoon, *J. Catalysis Today,* 123, 303–309 (2007).

[8] J.S. Jang, H.G. Kim, P. H. Borse and J. S. Lee, *Int. J of Hydrogen Energy,* 32, 4786–4791 (2007).

[9] U. Ghosh, *J. Human and Ecological Risk assessment*, 13, 276–285 (2007).

[10] W. Cho, S.H. Lee, W.S. Ju, Y. Baek and J.K. Lee, *J. Catalysis Today*, 98, 633–638 (2004).

[11] F.C. Lockwood, J.E. Niekerk and J.E. Van, *J. Combustion and Flame*, 103, 76–90 (1995).

[12] P. Towler and S. Lynn, *J. Chemical engineering communications*, 155, 113–143 (1996).

[13] A.M. Dunker, S. Kumar and P. A. Mulawa, *J. Hydrogen Energy*, 31, 473–484 (2006).

[14] K. Sakanishi, Z. Wu, A. Matsumura and I. Saito, *J. Catalysis Today*, 104, 94–100 (2005).

[15] A. Saario and A. Rebola, J. Fuel, 84, 359–369 (2005).

[16] W.P. Jones and J.H. Whitelaw,, *J. Combustion and Flame,* 48, 1–26 (1982).

[17] J. Warnatz, U. Maas, and R.W Dibble., "Combustion", Springer-Verlag, Berlin (2006).

[18] S.J. Brooks and J. B. Moss, *J. Combustion and Flame,* 116 (1999) 486–503.

[19] Z. Wen, S. Yun, M.J. Thomson, and M.F. Lightstone, *J. Combustion and Flame*, 135, 323–340 (2003).

[20] K. Bashirnezhad, M. Moghiman, I. Zahmatkesh, *Iran. J. Chem. Chem. Eng*., 26, 45–54 (2007).

[21] J.Y. Murthy and S.R. Mathur, AIAA-98-0860, January 1998.